peroxide:25% ammonia:water = 1:1:5, 80°C). A drop of poly-L-lysine (molecular weight 15,000 to 30,000, Sigma, Heidelberg) at a concentration of 1 mg/ml in water was applied to the gate and dried. The chamber was filled with leech Ringer (115 mM NaCl, 4 mM KCl, 1.8 mM $CaCl_2$, 10 mM tris-maleate, pH 7.4). A neuron was sucked several times into a wide glass pipette (tip diameter, 80 to 100 μm) to remove connective tissue and was transferred into the chamber. We attached the cell to a narrow pipette (tip diameter, 10 to 25 μm) by suction and pressed it gently onto the gate with a micromanipulator and a stereomicroscope. The micropipette was removed. The attachment was completed within a few minutes after addition of Ringer to the chamber as the coat of poly-L-lysine faded away. Measurements with the FET were started within a minute after attachment. After tests to record spontaneous activity, we impaled a microelectrode (tip diameter <1 μm). After completion of the measurements, the chip was cleaned with water and hot basic hydrogen peroxide and reused.

18. Bulk Si and source were kept at 2.7 V and the drain was kept at 0.7 V such that the source-drain voltage V_{DS} was −2 V as marked in Fig. 3E. The current was fed into a current-voltage converter. After amplification and filtering, the signal was digitized and read into a computer. All measurements were performed in the dark to avoid photocurrents. The neuron was impaled by a glass microelectrode filled with 3 M KCl and contacted with a Ag/AgCl electrode. It was connected to a voltage follower of standard design such that the membrane potential was measured at low impedance and current could be injected through the electrode. The signal was digitized and read into the computer.

19. We thank M. Brandstätter, V. Tegeder, F. Jäger, and S. Jäger, who helped in setting up the Si technology in our laboratory. Mask preparation was supported by the Abteilung Festkörperphysik, Universität Ulm. We thank E. Neher for critical reading of the manuscript. Generous grants of the Fond der Chemischen Industrie to P.F. are acknowledged.

20 December 1990; accepted 15 March 1991

Spectroscopic Observations of Bright and Dark Emission Features on the Night Side of Venus

J. F. Bell III,* D. Crisp, P. G. Lucey, T. A. Ozoroski, W. M. Sinton, S. C. Willis, B. A. Campbell

Near-infrared spectra of a bright and a dark thermal emission feature on the night side of Venus have been obtained from 2.2 to 2.5 micrometers (μm) at a spectral resolution of 1200 to 1500. Both bright and dark features show numerous weak absorption bands produced by CO_2, CO, water vapor, and other gases. The bright feature (hot spot) emits more radiation than the dark feature (cold spot) throughout this spectral region, but the largest contrasts occur between 2.21 and 2.32 μm, where H_2SO_4 clouds and a weak CO_2 band provide the only known sources of extinction. The contrast decreases by 55 to 65 percent at wavelengths longer than 2.34 μm, where CO, clouds, and water vapor also absorb and scatter upwelling radiation. This contrast reduction may provide direct spectroscopic evidence for horizontal variations in the water vapor concentrations in the Venus atmosphere at levels below the cloud tops.

Near-infrared (NIR) images and spectra of Venus acquired by Allen and Crawford (*1*) revealed that the night side of the planet was unexpectedly bright at wavelengths near 1.7 and 2.3 μm, in atmospheric windows between strong CO_2 and water vapor absorption bands. These authors concluded that this night-side radiation was produced thermally in the hot lower atmosphere of Venus. The bright-contrast and dark-contrast features were thought to be produced as this radiation passes through a higher, cooler, optically thin cloud region. Subsequent observations and theoretical analysis confirmed these conclusions. Allen (*2*) ratioed low-resolution spectra of bright and dark regions of the Venus night side and found that this ratio was almost independent of wavelength. This result implies that the agent that produces the dark features is a continuum absorber, such as the H_2SO_4 cloud droplets, rather than a gas. Kamp *et al.* (*3*) showed that the night side radiation could be completely accounted for by thermal emission from the pressure-broadened far wings of CO_2 and H_2O lines in the deep Venus atmosphere. Their results also showed that intensity contrasts as large as those observed on the night side could be produced by variations in the cloud optical depth of 20%. Crisp *et al.* (*4*) combined infrared images of Venus with Allen's spectra and spacecraft observations (*5*) and showed that the features were produced by horizontal variations in the optical depth of the middle or lower cloud deck at altitudes between 48 and 55 km. The feature rotation period at those levels was found to be about 6 ± 1 days, indicating equatorial east-west wind velocities of about 70 m/s. Bezard *et al.* (*6*) analyzed new high-resolution spectra of a bright region on the Venus night side and showed that the thermal emission in the 2.3-μm region originates primarily at levels above 8 bars (30 km), whereas the 1.74-μm radiation is produced at deeper levels. Their spectra placed new constraints on the concentrations of several important trace gases in the lower Venus atmosphere, including H_2O, CO, HCL, and HF. They also provided an independent confirmation of the enhanced D/H ratios observed by Pioneer Venus (7) and provided the first true detection of OCS in the Venus atmosphere.

New imaging and spectroscopic observations of the Venus night side were taken from a global network of observatories during January and February of 1990 to support the Galileo spacecraft Venus flyby. On 10 February 1990 UT the Galileo Near-Infrared Mapping Spectrometer (NIMS) was the first spacecraft instrument to take NIR images and spectra of the Venus night side. These data have better spatial resolution than the ground-based data, but severe limits on the data telemetry rate and on spacecraft tape recorder storage restricted the spatial, temporal, and spectral coverage of the NIR features.

To complement the Galileo NIMS experiment we conducted daytime spectroscopic observations of Venus from the National Aeronautics and Space Administration (NASA) Infrared Telescope Facility (IRTF) at Mauna Kea Observatory during 26 to 30 January 1990. This observing period was ideal for spatially resolved studies of the night side of Venus because passage of the planet through inferior conjunction less than 2 weeks before provided a relatively large disk (60 arc seconds) and a thin sunlit crescent (α = 155°). We used the Cooled-Grating Array Spectrometer (CGAS) to provide a spectral resolution between 1200 and 1500 in the 1.7- and 2.3-μm windows (*8*). The CGAS has a 2.7–arc second circular entrance aperture and yielded an effective spatial resolution of 550 km on the Venus night side. Because Venus was perilously close to the sun in the morning sky, we used a special telescope mask to prevent sunlight from striking the primary mirror (*9*).

We coordinated our spectroscopic observation program with a concurrent NIR imaging program lead by Sinton and co-workers at the University of Hawaii Air Force 61-cm telescope on Mauna Kea (*10*). Their images allowed us to acquire spectra of the darkest and brightest features on the Venus night side. A 2.36-μm NIR camera image acquired on the morning of 29 January 1990 UT showed a large (~5–arc second) hot spot on the Venus night side centered at

J. F. Bell III, P. G. Lucey, T. A. Ozoroski, B. A. Campbell, Planetary Geosciences Division, University of Hawaii, Honolulu,HI 96822 and Visiting Astronomers at the Infrared Telescope Facility, operated by the University of Hawaii under contract to the National Aeronautics and Space Administration.
D. Crisp, Jet Propulsion Laboratory and California Institute of Technology, Mail Stop 169-237, 4800 Oak Grove Drive, Pasadena, CA 91109.
W. M. Sinton, Institute for Astronomy, University of Hawaii, Honolulu, HI 96822.
S. C. Willis, Remote Sensing Lab, Mail Stop AJ-20, University of Washington, Seattle, WA 98195.

*To whom correspondence should be addressed.

16°N latitude (Fig. 1). We obtained two spectra of the hot spot and one of the cold spot during the short (4-hour) morning observing period.

The spectra were obtained in seven spectral intervals across the 2.2- to 2.5-μm region; each spectral interval has an eight-channel overlap with the adjoining interval. We observed α Lyr at an almost identical airmass as Venus and used its spectrum for atmospheric extinction and instrument response corrections and for flux calibration. The CGAS is not an optimum instrument for photometry [absolute photometric performance rarely exceeds 10% (*8*)], but because of the large contrast difference between bright and dark regions and the high NIR flux level from the Venus night side, this level of precision is adequate to identify the location and origins of the emission. The ratio of hot-spot and cold-spot spectra taken only 3 to 5 min apart exhibits a much higher precision than the absolute spectra because of the near complete cancellation of instrumental and terrestrial atmospheric effects.

Calibrated hot-spot and cold-spot spectra (Fig. 2) show several similar absorption features. The most prominent are the CO 2-0 fundamental bands at 2.29 to 2.34 μm and 2.35 to 2.45 μm, CO_2 bands at wavelengths shorter than 2.3 μm (*11*), and H_2O bands at wavelengths longer than 2.39 μm. In addition, OCS absorbs at wavelengths between 2.44 and 2.46 μm (*6, 11*). The overall shape of the cold-spot spectrum is almost identical to that of the spectra described by Allen (*2*) and Bezard *et al.* (*6*). The two hot-spot spectra have similar shapes and intensities, but their shapes differ substantially from those of the earlier spectra. For example, they are more than twice as bright as the spectrum of Bezard *et al.* (*6*) at wavelengths near 2.3 μm, but they have comparable intensities at 2.4 μm. This change in shape appears as a sharp change in contrast near 2.34 μm in the ratio of hot-spot to cold-spot spectra (Fig. 3). At wavelengths less than 2.34 μm, this ratio is about 5, but it decreases to about 3 beyond 2.34 μm.

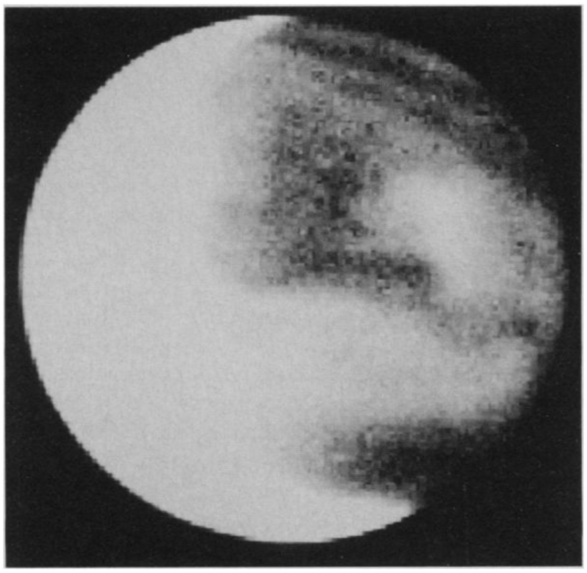

Fig. 1. K-band (2.2 μm) NICMOS near-infrared camera image of Venus obtained at 1710 UT 29 January 1990 from Mauna Kea (*10*). North is up and east is to the left. The bright, irregular region of the night side just east of the limb is the hot spot observed with CGAS. The cold spot is the dark region located 15 arc seconds (0.5 Venus radii) east of the hot spot.

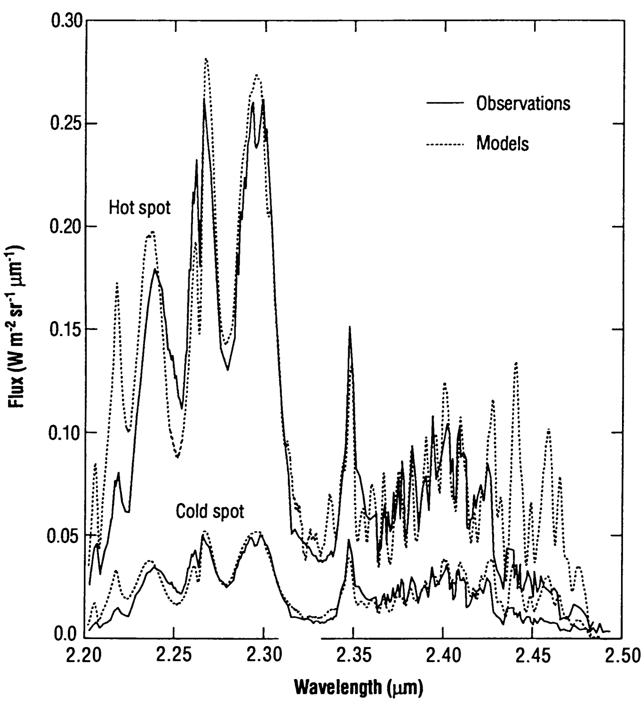

Fig. 2. Spectra of the hot spot and cold spot depicted in Fig. 1. The hot-spot and cold-spot spectra were compiled from seven independent spectral segments. Each segment consisted of 30 channels and had an 8-channel overlap with adjacent segments. The hot-spot flux is consistently greater than that from the cold spot, however the contrast is much greater at wavelengths less than 2.34 μm. The simulated hot-spot spectrum was produced with the use of the wet profile described in the text and a nominal cloud model (*19*) in which the optical depths of the mode-2′ and mode-3 particles were reduced by 60% (equivalent to a 22% reduction in the total Venus cloud optical depth). The dry profile (*6*) and the nominal cloud model (*19*) were used in the simulated cold-spot spectrum. The CO and OCS abundances for both spectra were taken from (*6*). Errors in the depth of the CO_2 absorption features at wavelengths shorter than 2.3 μm are caused by known errors in the strengths of weak CO_2 lines at these wavelengths (*11*). Water vapor and CO produce extinction primarily at wavelengths longer than 2.3 μm.

Because Allen (*2*) saw no large contrast changes near 2.34 μm, we conducted a series of tests to insure that this feature was not an artifact of our observing technique or data processing methods. Scattered sunlight could introduce a spurious blue slope in the hot-spot spectrum, but it could not produce a sharp contrast change like that seen in Fig. 3. Small tracking errors that allowed the hot spot or cold spot to slowly drift out of our aperture while the different spectral segments were being compiled could also produce contrast changes, but such changes would not be as sharp as those observed because the boundaries of the hot spot and cold spot are not sharp. A video tape of the television guider output shows no evidence for large, sudden drifts. Furthermore, there is no known reason why such errors would occur at the same wavelength in both hot-spot spectra. Tracking errors are of somewhat greater concern for the single cold-spot spectrum, but there is less reason to suspect its reliability because its shape is similar to all previously collected NIR spectra of the Venus night side. The process of combining the seven different spectral segments into a complete spectrum involves the use of poorly constrained scaling factors (*8, 12*), but it is unlikely that this process introduced the observed contrast change because this change occurs near the middle of a single segment, instead of near the end. In spite of this, we tested the reliability of our methods for combining these segments by using two completely independent methods. Both methods produced almost identical results for the hot-spot and cold-spot spectra.

The contrast change at 2.34 μm could have important implications for the composition of the deep Venus atmosphere. If the

Venus clouds are composed primarily of concentrated sulfuric acid droplets, the contrast change cannot be produced by the clouds because there are no known variations in the spectrum of sulfuric acid at these wavelengths (*13*). This spectral contrast change could be produced if the hot spot was associated with increased H_2O mixing ratios below the clouds. Water vapor absorbs strongly at wavelengths longer than 2.3 μm but produces little absorption at shorter wavelengths (*14*). Variations in the CO and OCS abundances at these levels could also contribute to the observed contrast change, but neither of these gases absorbs at all wavelengths where the contrast reduction is seen (*11*).

To quantify our results and to improve our understanding of the mechanisms that produce the spectrally dependent bright and dark feature contrasts on the night side of Venus, we used a numerical radiative-transfer model to simulate the observed spectra. Monochromatic gas absorption coefficients and optical depths were derived from a version of the line-by-line model (*15*). That model was modified for use in the high-temperature, high-pressure Venus atmosphere by addition of an explicit treatment of the sub-lorentzian shape of the pressure-broadened far wings of CO_2 and CO lines (*16*) and the super-lorentzian shape of water vapor lines (*17*), and by inclusion of pressure-induced CO_2 absorption bands (*18*). We obtained the thermal irradiance at the top of the vertically inhomogeneous Venus atmosphere by incorporating the monochromatic gas optical depths and aerosol optical properties into a version of the delta-Eddington-Adding program (*19*) that was modified by adding a thermal source function in each layer. We estimated the upwelling radiance at the top of the atmosphere from the computed irradiances by assuming that the radiance field at the top of the atmosphere was independent of zenith angle and dividing the irradiances by π.

The nominal input atmosphere includes absorption by four gases (CO_2, H_2O, CO, and OCS) as well as absorption and multiple scattering by clouds consisting of the four distinct sulfuric acid particle modes (1, 2, 2′, and 3) observed by the Pioneer Venus Cloud Particle Spectrometer Experiment (*20*). The nominal temperature and pressure profiles were taken from the Pioneer Venus Sounder Probe measurements (*21*). To simulate the hot-spot spectra, we modified the nominal vertical cloud structure derived by Crisp (*19*) by decreasing the optical depths of H_2SO_4 particle modes 2′ and 3 in the middle and lower clouds. The model atmospheres had 50 layers between the surface and an altitude of 100 km. These layers were almost equally spaced in the log of pressure. The CO_2 mixing ratios were set to 0.96 at all levels, and the CO and OCS mixing ratios were as in (*6*). Two different H_2O mixing ratio profiles were used. The wet profile was a simplified version of that inferred from Venera 13 and 14 measurements (*22*). It has water vapor mixing ratios that increase from 0.8 ppmv above 65 km, to 100 ppmv at 45 km, and then to 200 ppmv below 40 km. The dry profile (*6*) has 0.8 ppmv above 65 km, increasing to 40 ppmv of H_2O at all altitudes below 55 km.

The synthetic spectra were computed on a wavelength grid with a resolution of 0.01 cm^{-1} and then smoothed with a triangular slit function with a full width at half maximum of 4 cm^{-1} to simulate the CGAS results. The shape and amplitude of the computed spectra were sensitive to the particle size distribution assumed, but they were much less sensitive to the vertical structure of the clouds. A best fit to the observed hot-spot spectrum was produced by removing 60% of the mode 2′ and mode 3 particles from the middle and lower clouds (*23*). This constitutes about 22% of the total cloud optical depth. The best fit cold-spot model was produced with the use of the nominal cloud opacities described by Crisp (*19*).

A comparison between the observed and computed hot-spot and cold-spot spectra (Fig. 2) shows that the wet profile (*22*) produces a much better fit to the hot-spot spectrum, but it produces too much absorption at wavelengths longer than 2.34 μm for the cold-spot case. In contrast, the dry case (*6*) provides a good fit to the cold-spot spectrum, but does not produce enough attenuation at wavelengths longer than 2.34 μm for the hot-spot case. These conclusions are reinforced by the comparison between the ratios of observed and computed hot-spot and cold-spot spectra (Fig. 3). The best fit to the observations is produced by a model atmosphere in which the amount of water vapor decreases as cloud abundance increases.

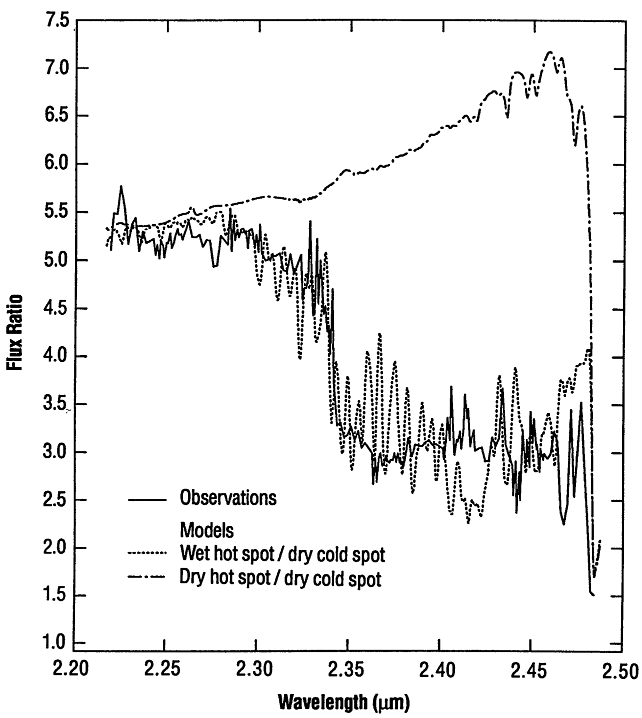

Fig. 3. The ratio of the observed hot-spot and cold-spot spectra (solid line) is compared to ratios of synthetic spectra for wet and dry model atmospheres (see Fig. 2). The observed radiance emitted by the hot spot is about 55 to 65% greater than the cold spot shortward of 2.34 μm. The wet and dry hot-spot models are identical in all respects, except for the water vapor profiles. Oscillations in the simulated spectral ratio longward of 2.34 μm are due to uncertainties in the vertical distribution of H_2O.

These observations and simulations may provide direct spectroscopic evidence for the presence of large horizontal variations in H_2O in the deep Venus atmosphere. Our hot-spot spectra also yield H_2O abundances as large as those measured by the Pioneer Venus and Venera descent probes. Earlier NIR spectra indicated that H_2O abundances were 20 to 40% of that indicated by the spacecraft data; this difference caused some concern that the different techniques may not be measuring the same phenomenon. The apparent relation between bright regions and high water amounts could be explained if the bright regions are produced by sedimentation of H_2SO_4 cloud particles and subsequent evaporation. The H_2SO_4 vapor would then thermally dissociate to form H_2O and SO_3 in the hot atmosphere below the clouds. The lifetime of water-rich regions would be limited by horizontal mixing associated with the strong vertical shear in the east-west winds below the clouds, and perhaps by other processes.

We have too little information to test this simple model fully (*24*). Crisp *et al.* (*25*) have obtained ratios of narrow-band images of Venus at 2.24 and 2.4 μm that show small, spatially dependent contrast variations, but their analyses of these images indicates that H_2O variations are much smaller than those seen here, and they are not well correlated with either feature brightness or latitude. The spatially resolved spectra collected by the Galileo NIMS experiment could help to determine the spatial relationship of the NIR features and the trace gas abundances in the lower Venus atmosphere.

The apparent presence of spatially varying H_2O abundances below the clouds has a variety of implications for studies of the deep Venus atmosphere. For example, the spatial distribution of wet and dry regions must be known to estimate the total water budget of the lower Venus atmosphere. The water budget, in turn, affects the efficiency of the atmospheric greenhouse mechanism that maintains the high surface temperatures. Both water vapor and clouds play an important role in this greenhouse by blocking thermal emission in spectral windows between CO_2 bands (*26*). Abundances of H_2O as large as those inferred from our hot-spot spectra, along with an unbroken cloud deck as thick as that used for our cold-spot model are assumed in current greenhouse models to yield the observed surface temperatures (730 K). Thus other greenhouse absorbers or other radiative processes that are not currently included in those models may be needed to account for these high temperatures in consideration of the lower water abundances of cold-spot regions and the lower cloud abundances of hot-spot regions that we have observed.

REFERENCES AND NOTES

1. D. A. Allen and J. W. Crawford, *Nature* **307**, 222 (1984).
2. D. A. Allen, *Icarus* **69**, 221 (1987).
3. L. W. Kamp, F. W. Taylor, S. B. Calcutt, *Nature* **336**, 360 (1988).
4. D. Crisp *et al.*, *Science* **246**, 506 (1989).
5. A. P. Ingersoll *et al.*, *Adv. Space Res.* **7**, 343 (1987); D. Crisp, A. P. Ingersoll, C. E. Hildebrand, R. A. Preston, *ibid.* **10**, 109 (1990).
6. B. Bezard, C. DeBergh, D. Crisp, J.-P. Maillard, *Nature* **345**, 508 (1990).
7. J. H. Hoffman, R. R. Hodges, T. M. Donahue, M. B. McElroy, *J. Geophys. Res.* **85**, 7882 (1980); V. I. Oyama *et al.*, *ibid.*, p. 7891.
8. A. Tokunaga, L. Bergknut, K. Sellgren, *The Cooled Grating Array Spectrometer User's Manual* (NASA Infrared Telescope Facility, Mauna Kea, HI, 1990).
9. This full-aperture (3.0-m) mask had a 1.22-m circular hole that was placed off center, between the telescope's secondary mirror supports, to produce a completely unobstructed aperture. The mask reduced the light collection area of the IRTF by a factor of 6, but this was not a problem because the night side of Venus is relatively bright (visual magnitude ≈ 7). The unobstructed aperture also reduced the amount of light that could be scattered from the bright sunlit crescent onto the night side by eliminating the diffraction from the telescope's secondary mirror support structure.
10. W. M. Sinton, P. Kalas, K.-L. Hodapp, R. Wainscoat, B. Ragent, D. Crisp, *Bull. Am. Astron. Soc.* **22**, 1053 (1990); D. Crisp *et al.*, *ibid.*, p. 1053.
11. J. H. Park *et al.*, *NASA Ref. Publ. 1188* (1987); L. S. Rothman *et al.*, *Appl. Opt.* **26**, 4058 (1987). It should also be noted that the high-temperature CO_2 spectrum is poorly known in the NIR at this time.
12. J. F. Bell III, "Venus CGAS Data Reduction" (Hawaii Institute of Geophysics Internal Report, Honolulu, 1990).
13. K. F. Palmer and D. Williams, *Appl. Opt.* **14**, 208 (1975).
14. The presence of water vapor in Earth's atmosphere impairs studies of water vapor at levels above 1 bar in the Venus atmosphere because the Venus water lines are strongly blended with their much stronger telluric counterparts. The H_2O in the deep atmosphere of Venus produces much larger effects on emission spectra because the pressure-broadened far wings of water lines that are formed at pressures greater than 1 bar are not hidden by their telluric counterparts.
15. D. Crisp, *J. Geophys. Res.* **95**, 14577 (1990).
16. M. Fukabori, T. Nakazawa, M. Tanaka, *J. Spect. Quan. Rad. Trans.* **36**, 265 (1986); *ibid.*, p. 283.
17. M. E. Thomas and R. J. Nordstrom, *Appl. Opt.* **24**, 3526 (1985).
18. J. F. Moore, *NASA–Goddard Space Flight Center Rep. X-630-72-48* (1971).
19. D. Crisp, *Icarus* **67**, 484 (1986).
20. R. G. Knollenberg and D. M. Hunten, *J. Geophys. Res.* **85**, 8039 (1980).
21. A. Seiff *et al.*, *ibid.*, p. 7903.
22. V. I. Moroz, in *Venus*, D. M. Hunten, L. Colin, T. M. Donahue, V. I. Moroz, Eds. (Univ. of Arizona Press, Tucson, 1983), pp. 45–68.
23. This choice was motivated by a comparison between the Pioneer Venus and VEGA entry probe cloud-particle spectrometer measurements. The VEGA lander saw many fewer large particles than the Pioneer Venus large probe (*20*) in the middle and lower clouds [B. E. Moshkin *et al.*, *Sov. Astron. Lett.* **12**, 36 (1986)].
24. The enhanced SO_3 abundance predicted by this scheme cannot be tested because the absorption by SO_3 is not well documented at these wavelengths. Also, this data set alone cannot be used to test the apparent relation between H_2O and cloud amount because all of our 2.3-μm spectra were taken from the same hot and cold spots.
25. D. Crisp *et al.*, in preparation.
26. J. B. Pollack, O. B. Toon, R. Boese, *J. Geophys. Res.* **85**, 8223 (1985).

27. We thank C. Lindsey for the use of his Solar filter mask (which became our Venus mask) and telescope operators B. Golisch and G. Koenig, as well as the rest of the day crew and support scientists of the Infrared Telescope Facility, for their assistance. We also thank A. Tokunaga and T. Brooke for invaluable assistance with CGAS data reduction software. W.M.S. is indebted to K.-L. Hodapp and J. Rayner and their infrared array engineers and technicians and B. Ragent, R. Wainscoat, S. Ridgway, and P. Kalas, who collaborated in making the imaging observations. This work was supported by grants from the NASA Planetary Astronomy and Planetary Atmospheres program to the Jet Propulsion Laboratory, California Institute of Technology, and the University of Hawaii. University of Hawaii Planetary Geosciences Division Publication #645.

17 January 1991; accepted 3 April 1991

Identification of the DNA Binding Site for NGFI-B by Genetic Selection in Yeast

THOMAS E. WILSON, TIMOTHY J. FAHRNER, MARK JOHNSTON, JEFFREY MILBRANDT*

An in vivo selection system for isolating targets of DNA binding proteins in yeast was developed and used to identify the DNA binding site for the NGFI-B protein, a member of the steroid–thyroid hormone receptor superfamily. The feasibility of the technique was verified by selecting DNA fragments that contained binding sites for GCN4, a well-characterized yeast transcriptional activator. The DNA binding domain of NGFI-B, expressed as part of a LexA–NGFI-B–GAL4 chimeric activator, was then used to isolate a rat genomic DNA fragment that contained an NGFI-B binding site. The NGFI-B response element (NBRE) is similar to but functionally distinct from elements recognized by the estrogen and thyroid hormone receptors and the hormone receptor–like proteins COUP-TF, CF1, and H-2RIIBP. Cotransfection experiments in mammalian cells demonstrated that NGFI-B can activate transcription from the NBRE with or without its putative ligand binding domain.

EXPRESSION OF EARLY RESPONSE genes is rapidly and transiently induced in response to various stimuli, including growth factors. These genes often encode transcriptional regulatory proteins [for example c-*fos* and c-*jun* (*1*)] and are thought to activate or repress genes appropriate to the changing cellular environment or to the newly differentiated state. However, the target genes of most mammalian early response genes have not been identified, so their specific functions in cellular differentiation are unknown.

NGFI-B is an early response gene that is induced by nerve growth factor (NGF) in the rat pheochromocytoma cell line PC12 (*2, 3*). This neural crest-derived cell line responds to NGF by differentiating into a postmitotic cell type with neuronal characteristics (*4*). Sequence analysis shows that NGFI-B shares similarity with the steroid–

T. E. Wilson, T. J. Fahrner, J. Milbrandt, Division of Laboratory Medicine, Departments of Pathology and Internal Medicine, Washington University School of Medicine, St. Louis, MO 63110.
M. Johnston, Department of Genetics, Washington University School of Medicine, St. Louis, MO 63110.

*To whom correspondence should be addressed.